

# PIV investigation of internal cooling channels for gas turbines, with 45 degrees inclined ribs

by

R. Garcia Casado<sup>(1)</sup>, M. Thierry<sup>(2)</sup>, R. Fedrizzi<sup>(3)</sup>, A. di Sante<sup>(4)</sup> and T. Arts<sup>(5)</sup>

von Karman Institute for Fluid Dynamics

Turbomachinery and Propulsion Department

Chaussée de Waterloo 72, B-1640 – Rhode Saint Genese; Belgium

[www.vki.ac.be](http://www.vki.ac.be)

<sup>(1)</sup> [garciaca@vki.ac.be](mailto:garciaca@vki.ac.be)

<sup>(4)</sup> [disante@vki.ac.be](mailto:disante@vki.ac.be)

<sup>(5)</sup> [arts@vki.ac.be](mailto:arts@vki.ac.be)

<sup>(2)</sup> [thierry@vki.ac.be](mailto:thierry@vki.ac.be)

<sup>(3)</sup> [roberto.fedrizzi@ing.unitn.it](mailto:roberto.fedrizzi@ing.unitn.it)

## ABSTRACT

The object of this study is to characterize the aero-thermal performance of a rectangular turbine blade cooling channel for gas turbines equipped with turbulence promoters, square section ribs, inclined at 45 degrees with respect to the main flow direction. With this aim, a P.I.V investigation of the flow field within an inter-rib space inside four cooling channel models has been done. The presence of the ribs aims at ripping the boundary layer in order to increase the turbulence level and thus enhance the heat transfer between the channel walls and the coolant air. Four different configurations are reported, based in two parameters: the inter-rib distance, normalized with respect to the rib height ( $s/h=7.5$  and  $s/h=15$ ), and the presence of ribs on one or on two opposed walls. The measurements were carried out for a Reynolds number of 40000, representative for this kind of passages. Using Particle Image Velocimetry, mean flow field patterns are displayed along four mutually perpendicular planes in the inter-rib space, to present the three dimensional behavior of the flow in the projected measurement planes. Fluctuating flow features are reported for every measurement plane. Liquid Crystal Thermography was used for the thermal measurements on the ribbed walls, giving Nusselt number contours plots for every configuration. The link between the aerodynamic field and cooling capability is shown by superposing the obtained streamlines in a plane parallel to the inter-rib wall on the Nusselt contours. The acquired data are also a contribution to a database for testing numerical codes.

## LIST OF SYMBOLS

$s$  = rib to rib pitch distance

$h$  = rib height

$TSFC$  = Thrust Specific Fuel Consumption

$\dot{m}$  = mass flow rate

$F$  = thrust

$C_p$  = specific heat at constant pressure

$T_1$  = inlet compressor temperature

$T_{01}$  = total inlet compressor temperature

$T_{03}$  = total inlet compressor temperature

$p_c$  = compressor pressure ratio

$\gamma$  = ratio of specific heat of a gas

$Q_f$  = fuel flow rate

$\dot{m}_a$  = air mass flow rate

$D_h$  = hydraulic diameter

$x, y, z$  = coordinates in streamwise, vertical and lateral direction  
 $u, v, w$  = streamwise, vertical and lateral mean velocity components  
 $u', v', w'$  = streamwise, vertical and lateral fluctuating velocity components

$$rms = \sqrt{\langle (u - u')^2 \rangle} \text{ for the axial velocity component}$$

$Re$  = Reynolds number

$Pr$  = Prandtl number

$Nu$  = Nusselt number

$u_0$  = bulk velocity

$\Delta t$  = laser pulse separation time

## LITERATURE SURVEY

Since more than a decade, studies about blade cooling had been carried out at *von Karman Institute*. The most recent items are a VKI *Lecture Series 2000-03 "Aero-thermal performance of internal cooling systems in turbomachines"* [19] and the PhD Thesis of Çakan "Aero-thermal investigation of fixed rib-roughened internal cooling passages" (*Universite Catholique de Louvain and VKI*) [3], and Casarsa "Aerodynamic Performance of a fixed rib-roughened internal cooling passage" (*Universita degli Studi di Udine and VKI*) [4].

The article "Comparison of heat transfer augmentation techniques" (*Ligrani et al. AIAA Journal Vol 41, No. 3 March 2003*) [12] shows a wide compilation of cooling techniques, including a section for internal cooling channels equipped with turbulence promoters. In this article, a high number of references are available on the topic. Referenced papers had been also used for this investigation.

About Particle Image Velocimetry, also a large amount of information is available on the literature, but the authors had been focused on the book "Particle Image Velocimetry, A Practical Guide" (*Raffel et al., Springer*) [18], and inside VKI, the PhD thesis of Scarano "Particle Image Velocimetry, development and application" (*Universita degli Napoli Federico II and VKI*) [8]. Other papers on this topic had been referenced along this article too.

## 1. INTRODUCTION

One of the main parameters that designers can vary in order to increase the thermodynamic efficiency of a gas turbine, quantified e.g. by the *Trust Specific Fuel Consumption*, is the turbine inlet temperature  $T_{03}$  (*Equation 1*). Nowadays, values over 2100 K are achieved, exceeding by far the melting temperature of the alloys used for inlet guide vanes and rotor blades. The need for cooling these components in the first stages of the turbine is therefore mandatory in order to achieve a safe operation of these components. For aeronautical applications, a combination of internal and external air cooling techniques is applied, using air bled from the compressor (*Figure 1*). The presence of ribs inside the cooling channels increases the turbulence level by ripping periodically the boundary layer, enhancing the forced convection heat transfer process. The penalty for the presence of the turbulators is the increase of the pressure drop along the channel. A compromise between forced convection effect and pressure drop must be achieved by the designer.

$$TSFC = \frac{\dot{m}}{F} = \frac{C_p \cdot \left( \frac{T_{03}}{T_1} - \frac{T_{01}}{T_1} \cdot P_c^{1-\frac{1}{\gamma}} \right) \cdot T_1}{Q_f \left( \frac{F}{\dot{m}_a} \right)} \quad \text{Equation 1.}$$

The scope of this research work is to characterize the aero-thermal behavior of the flow inside a turbine blade rectangular internal cooling channel, with one or two opposed ribbed walls. The turbulence promoters are square section ribs inclined at 45° with respect to the mean flow direction, introducing a blockage ratio of 10% for every ribbed wall. These ribs are placed on the large walls of the rectangular channel. Four configurations, varying the pitch to rib-height ratio ( $L/h=7.5$  and  $L/h=15$ ) for both one and two ribbed walls cases, are presented.

The main objectives are to describe the mean and fluctuating flow features in the inter-rib space relevant for the development of the design and analysis tools, and to explain the cooling performance of this highly three-dimensional flow.

In order to have a detailed view of the 3D flow field between two consecutive ribs, measurements within four mutually perpendicular planes were carried out, by means of Particle Image Velocimetry, into a scaled up glass model of a turbine blade internal cooling channel. These measurements were done respecting geometrical and flow similarity conditions with respect to a real case. To have a detailed view of the planes perpendicular to the inter-rib wall, the reference system was changed, to allow optical accessibility to this area of capital interest in the heat transfer process. Instead of being aligned with the main flow direction, as would be best suited for P.I.V. measurements, it is aligned with the rib direction. Thus, the perpendicular planes will not show the flow main direction, but a projection of the flow on the new reference axis (*Figure 4*). The data processing tool (*W.I.D.I.M.*) provided both mean and *rms* velocity components [8].

The contour maps of Nusselt number distribution for the inter-rib space were measured using encapsulated liquid crystals, painted on a model similar to the one used for the P.I.V. measurements. This second model was heated respectively on one or on two walls, depending on the measured configuration. The heat transfer results are only from convective effects, due to the insulating effect of the Plexiglas walls and ribs. The effects of radiation and heat conduction along the walls and ribs were not taken into account. The fact that the aerodynamic measurements were taken under isothermal conditions may neglect buoyancy effects, but even though, due to the low temperature in the heated model (around 330 K) these effects are not considered to be of importance. Other effects that the stationary channels do not take into account are the Coriolis forces that act in the rotating turbine blades, changing drastically the flow patterns.

Because of the directional effects promoted by the inclined ribs, the velocity field shows a strong three-dimensional character. Analyzing the experimental data, a non-symmetrical rib guided recirculating structure stands out as one of the main characteristics of the flow, being of capital importance in the heat transfer process. Reattachment lines and additional vortical structures present in the mean flow are also reported. The flow pattern differs significantly for the two different pitch to rib-height ratios, but not for the cases of one and two ribbed walls, whereas the heat transfer distribution does. The aerodynamic data are compared with the available inter-rib wall heat transfer distributions by superimposing the streamlines on the Nusselt number contours.

The acquired data are also accumulated to enlarge and improve a database used as numerical code test bench.

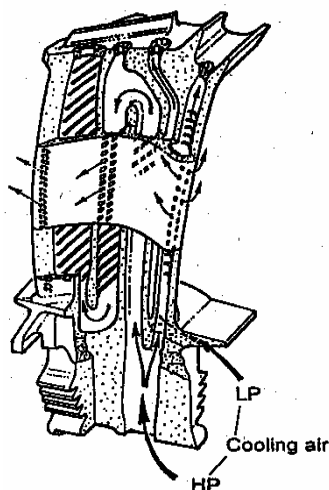


*Figure 1. Internal passages in a rotor blade*

## 2. EXPERIMENTAL SET-UP AND TECHNIQUES

### 2.1 Experimental Set-up

The stationary wind tunnel was constructed with the aim of performing the aerodynamic measurements using P.I.V.. Thus, the walls, including the ribbed ones, are in glass providing full optical access for the laser beams and the camera to the measurement areas. The entrance section top wall has a Plexiglas removable part, where pressure taps are drilled to control static pressure and mass flow, as well as a hole to allow the introduction of a hot wire probe, to measure the entrance flow field.

A sketch of the wind tunnel is shown in the *Figure 2*. The turbulence promoters are square section ribs, inclined at 45 degrees with respect to the direction of the main flow. The blockage introduced by the presence of the ribs,  $h/D_h$ , is 10% for every ribbed wall. The distance between ribs can be varied between  $15h$  and  $7.5h$ .

To be consistent with the previous works done at VKI by Thierry [1] and Fedrizzi [2] for the heat transfer distribution, the measurement section is placed after the 5<sup>th</sup> rib for  $l/h=7.5$  and after the 8<sup>th</sup> rib for  $l/h=15$ . From this pitch the flow behavior is considered periodic, based on previous studies done at VKI by Çakan [3]. The ribs in the measurement area are in brass, which when correctly polished, reflects properly the laser light and increase the total amount of light close to the rib walls.

The entrance to the channel is a convergent duct with a rectangular section. The reason is that the seeding distributor available at VKI, used to distribute uniformly the oil tracer particles necessary for the P.I.V. measurements, has a higher section than the one of the test channel.

At the entrance of the channel, a honeycomb was installed to assure a uniform inlet flow field. The influence of the seeding distributor in front of the channel has been studied by Casarsa [4], and is considered for the Reynolds number selected in this work with a correction factor of an increase 10% on the bulk velocity. The air is aspirated through the channel by a blower, located downstream of the test section. In order to limit the perturbations induced by the impeller in the flow, a settling chamber has been placed between the blower and the test section.

The working conditions of the facility are in geometrical and flow similarity with previous measurements done at VKI, and in similarity with the working conditions of the real cooling channels for turbine blades. These are a Reynolds number based on the hydraulic diameter ( $D_h$ ) and bulk velocity ( $u_0$ ) of  $Re=40000$ , and air at ambient conditions ( $Pr=0.7$ ).

The main difference between the channel used for the P.I.V. and the one used for the heat transfer measurements is that for the last one, the ribbed walls were heated in order to be able of simulate the heat transfer. Since the Reynolds number used is high enough to be considered as turbulent, the natural convection can be assumed to be negligible.

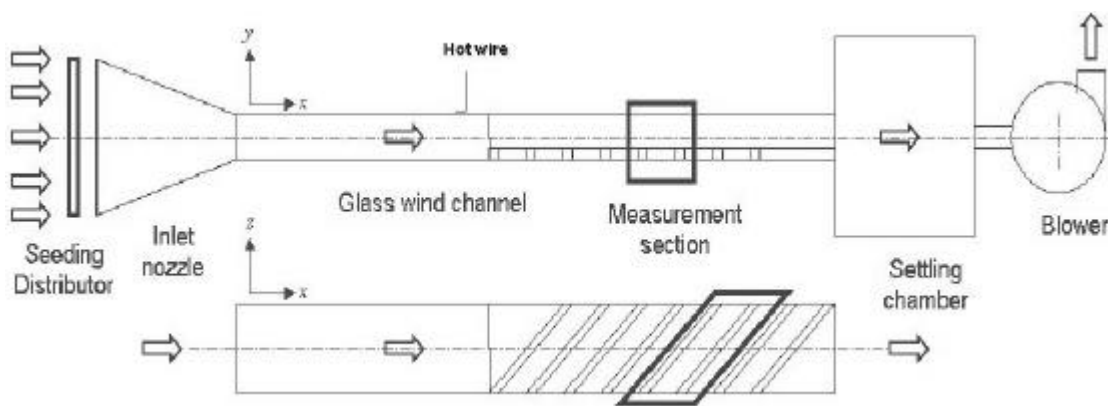


Figure 2. Experimental Set-Up

## 2.2 Experimental Techniques

### Particle Image Velocimetry

In order to characterize the flow in the ribbed area, Particle Image Velocimetry was the selected tool. The setup scheme is shown in *Figure 3*. The P.I.V. system is made of:

- \* A *B.M.I.* Nd:Yag laser.
- \* A *C.C.D. SensicamPCO* digital video camera.
- \* A data acquisition system.
- \* A synchronizer between the laser trigger and the acquisition by the video camera.
- \* Cylindrical and spherical lenses to convert the laser beam in a laser sheet.
- \* An oil smoke generator for the tracer particles.

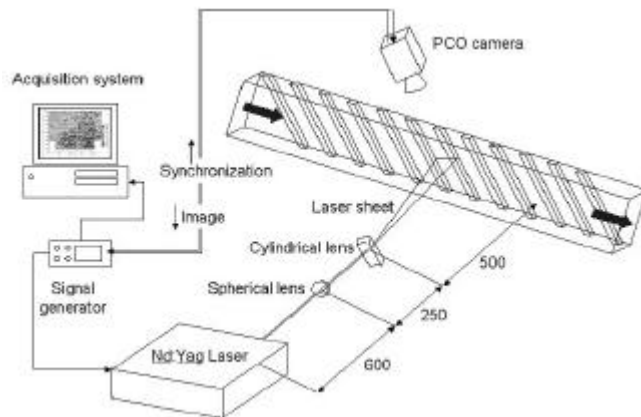


*Figure 3. Particle Image Velocimetry Set-Up*

The Nd:Yag laser emits green light from two cavities with a wavelength,  $\lambda = 532 \text{ nm}$ . Both cavities were used at constant double pulse rate with a frequency of  $8.1 \text{ Hz}$ , synchronized with the  $4.1 \text{ Hz}$  from the digital camera. A separation time  $\Delta t$  of  $15 \mu\text{s}$  was set between both laser pulses.

The *C.C.D.* digital video camera was a *SensicamPCO* unit with a resolution of  $1280 \times 1024 \text{ pixels}$ . The data acquisition software was the *SensiControl 4:03* by *PCO* provided with the camera. An objective of  $35 \text{ mm}$  of focal length was set on the camera with an aperture factor of 8. This allows recording and treating properly the images from the illuminated flow field. Thus, a resolution of around  $14000 \text{ pixel/m}$  was achieved for every measurement zone.

To synchronize the laser and the camera, a Stanford generator, *DG 535 four channel digital delay/pulse generator*, from *Stanford Research Systems Inc.* was used. The signals coming from the generator are completed with the signals coming from the camera and the laser cavities. This procedure works since the camera works at half the frequency of the laser.

A cylindrical lens of negative focal length equal to  $-19 \text{ mm}$  and a spherical one of  $130 \text{ mm}$  set behind the cylindrical were used in order to obtain the adequate laser sheet thickness between  $0.5$  and  $1 \text{ mm}$ .

The smoke generator was a Laskyn nozzle VKI smoke generator type. A plate warms up the oil contained in the tank to a temperature of around  $180^\circ\text{C}$ , evaporating it. By means of some valves and pressurized air, the evaporated oil is driven into the channel trough the inlet nozzle. The final size of the oil droplets is about  $1 \mu\text{m}$ . The value of the pressure set for the seeding generator was fixed at  $2 \text{ bar}$ .

The location of the measured planes can be seen in the sketch in *Figure 4*. The origin of the coordinate system is located at the downstream intersection of the first downstream rib surface with the lateral wall. The horizontal plane,  $1xz$  ( $y/h=0.16$  for both  $l/h=7.5$  and  $l/h=15$ ) will show the behavior of the flow in the inter-rib area, as close as possible to the bottom wall, while the three planes  $1xy$  ( $z/h=0$  for both  $l/h=7.5$  and  $l/h=15$ ),  $2xy$  ( $z/h=8.5$  for  $l/h=7.5$  and  $z/h=6$  for  $l/h=15$ ) and  $3xy$  ( $z/h=17$  for  $l/h=7.5$  and  $z/h=12$  for  $l/h=15$ ) will show the flow field projection at different positions perpendicular to the ribbed wall and also perpendicular to the ribs. In order to have a good spatial resolution, all

analyzed flow regions was split in 5 or 9 parts for the horizontal planes  $1xz$ , and 2 or 4 parts for the planes  $1xy$ ,  $2xy$  and  $3xy$ , for the configurations  $l/h=7.5$  and  $l/h=15$  respectively.

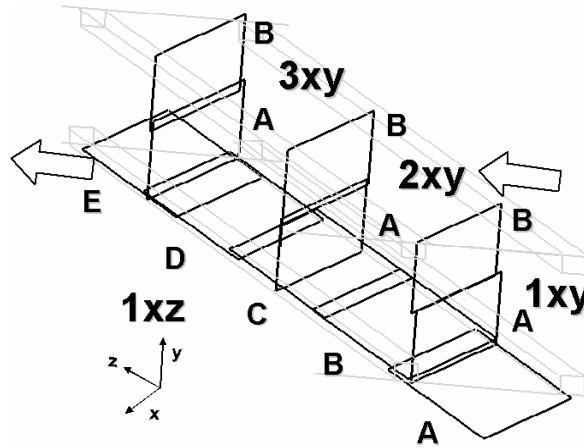


Figure 4. P.I.V. Measurement zones  $l/h=7.5$

To ensure the correct convergence of the statistical quantities, such as mean and *rms* velocities, 1000 pairs of images were acquired. The approach proposed by Riethmuller and Lourenço [5] was used to quantify the number of taken images. The maximum level of turbulence in the flow field, measured by means of hot-wire anemometry, was found in the streamwise velocity component, showing values up to 50% of the bulk velocity. From a preliminary study, it was shown that more than 95% of the measurements points present a level of fluctuation below 25%. With this value, 1000 samples are far above the limitation to give a time-averaged flow field with a 95% confidence level and a limited error on the mean velocity (5%) value and on its *rms* (5%) over the complete measurement domain. All P.I.V. images were processed using *W.I.D.I.M.*, software developed at VKI by Scarano and Riethmuller [6, 7, and 8]. All the data were processed using a  $48 \times 48$  pixels first interrogation window, one single step of window size refinement and 50% of window overlapping. Window distortion was used for each step of the refinement procedure. Finally, a Gaussian peak fitting was adopted to perform the sub-pixel interpolation. These settings result in a final window size of  $12 \times 12$  pixels, giving 9100 displacement vectors in each measurement area. The velocity fluctuations and normal stresses are normalized with the mean bulk velocity  $u_0$  calculated from the inlet velocity profiles for every configuration. Using the Kline and McClintock [9] analysis, the uncertainty on the instantaneous velocity was estimated to be less than 6%, based on the  $u_0$ .

#### Thermochromatic Liquid Crystals

T.L.C. Thermography was the method used at VKI to investigate the temperature distribution on the walls of internal cooling channels models [1, 2, 3, 10, 11, and 14]. Cholesteric liquid crystals are arranged in a twisted molecular structure, which gives them special optical properties. The path of the light in the material proceeds into two directions: a part of it, nearly 50%, is transmitted through the material; the rest is diffracted from the symmetric liquid crystals planes. The diffraction from parallel planes interferes constructively at a predominant wavelength, which depends on the pitch of the helical molecules and on the direction of the incoming light. For this type of crystals, the molecule pitch is a function of the temperature within a certain predefined range. The diffracted wavelength light is in the domain of the visible light.

In order to have an unambiguous sensation of the diffracted light, a C.C.D. camera acquires the image and software analyses the colors characteristics. The used method is based on the intensity information recorded, determining the different isothermal lines. It fully excludes human's color sensation through the use of optical band pass filters. By means of a calibration procedure, the wavelength diffracted by the liquid crystals can be related to a precise temperature. As the image is observed through a sharp band-pass filter, the intensity of the light becomes maximal around the temperature at which the peak wavelength of the light coincides with the maximum wavelength of the transmittance function of the band pass filter. This temperature is specified for each filter through a calibration (Çakan [3]). Although the isothermal lines were traced almost independently from any human judgment, only a finite number of isothermal lines can be provided at a time. Moreover, as only the low wavelength bands are sharp and thin enough to represent a line on the acquired image, the filters relative to the narrow bands have to be used. To cover the entire area of interest, the heating has to be varied many times so that traced colors move to different locations. A black and white camera can be used in this case as the hue and intensity information of the color are discarded.

For the steady state method used in this research, the liquid crystals are sprayed on the inside of a transparent and insulating external wall of the channel. With this purpose, an airbrush is used as it allows thin and uniform coating to be achieved. A layer of black paint, sprayed on the background of the T.L.C. layer, absorbs the light that is not diffracted by the liquid crystals. The steady method expects a uniform heat flux be realized between heated walls and main flow. The heat is supplied by passing current through a conducting inconel sheet bonded on the measurement surface (*Figure 5*). This material has a high electrical resistance, so that it remains almost constant even if the surface temperature changes slightly from point to point. This also brings to a steady heat flux provided by the wall to the flow. The thickness of the layers placed on the wall has also to be controlled carefully in order to minimize the Biot number of the composite layer and so reduce the lateral conduction.

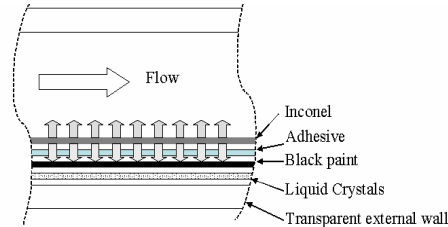


Figure 5. Liquid Crystals heated wall's layers sketch

### 3. RESULTS

#### 3.1 Inlet conditions

A hot wire probe was used in order to obtain the velocity and the turbulence intensity profiles at the inlet of the ribbed part of the channel (13  $D_h$  downstream of the channel inlet). Measuring these profiles ensures that the experiments are performed at similar flow conditions than the ones related to heat transfer. The local static pressure was measured with three pressure tabs, drilled one in. To control the Reynolds number, the pressure inside the channel was continuously checked by means of a water column. A correction factor for the bulk velocity of 1.1 was used to adequate this velocity because of the losses introduced by the presence of the honeycomb at the inlet of the channel. The difference was set between 5 and 6.1  $mmH_2O$  for the configurations  $l/h=7.5$  and  $l/h=15$  respectively. The precision of the water column was 0.1  $mmH_2O$ , and the uncertainty is about 3 %.

At this position, the flow was found to be turbulent but not fully developed (*Figure 6*). The boundary layer thickness is around 30% of the channel height. No significant difference can be appreciated between the profiles for both one and two ribbed walls configurations.

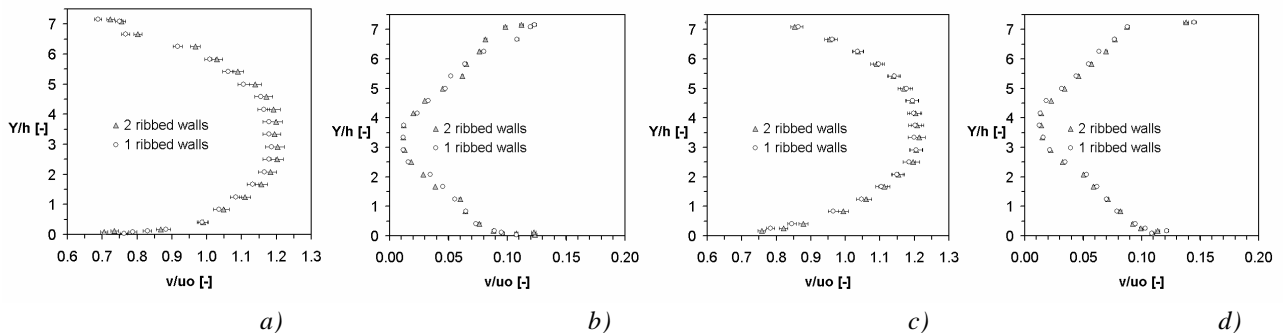


Figure 6. Inlet profiles

- a) Non dimensional inlet velocity profiles ( $l/h=7.5$ )    b) Non dimensional inlet turbulence profiles ( $l/h=7.5$ )  
c) Non dimensional inlet velocity profiles ( $l/h=15$ )    d) Non dimensional inlet turbulence profiles ( $l/h=15$ )

### 3.2 Aerodynamic behavior

Pitch to rib height ratio 7.5

A three dimensional reconstruction of the flow field for both configurations  $l/h=7.5$  is shown in the *Figure 7 a) and b)* for one and two ribbed walls respectively. The three dimensional flow behavior can be appreciated at first sight from both pictures. The unique symmetry yields in the *Figure 7 a)* due to the existence of opposed parallel ribs. No symmetry plane is identified for the single ribbed wall case, *Figure 7 b)*.

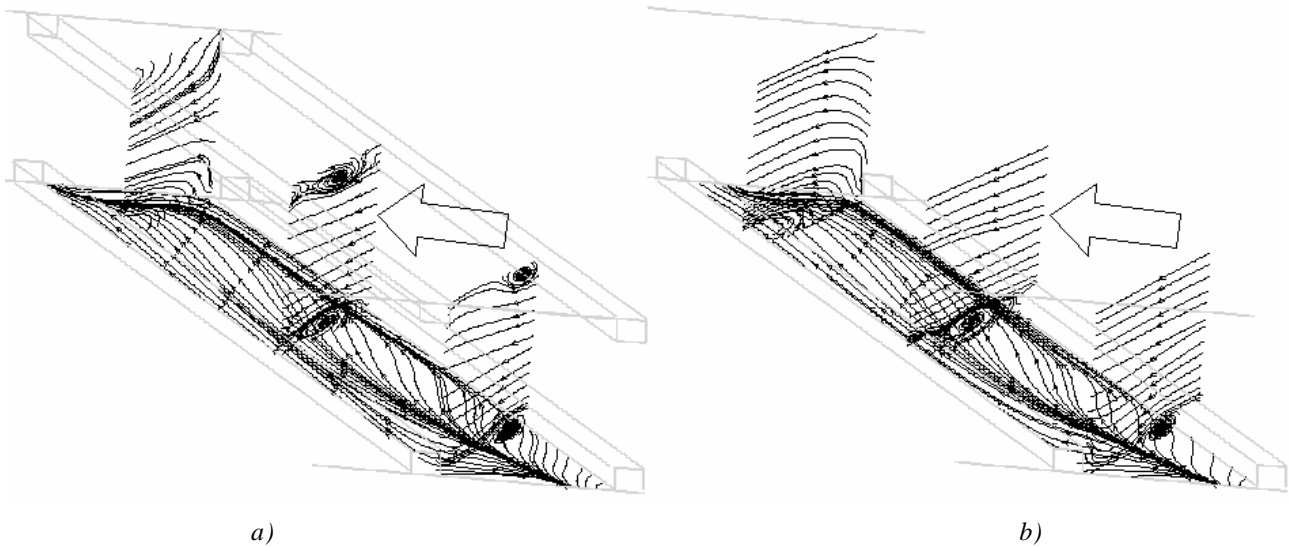


Figure 7. Inter-rib flow field projection  $l/h=7.5$

a) Two ribbed walls

b) One ribbed wall

For both one and two ribbed walls configurations, the flow strongly guided by the ribs inclination. This can be seen in the interstice between two successive ribs. Along the near inter-rib wall area, the coolant air flows from the upstream lateral wall towards the downstream one. A recirculating structure is created after the flow separation downstream of the first rib. This nonsymmetrical structure starts from the intersection of the upstream rib with the upstream sidewall. At this position, the flow is confined in this corner. The streamtracers show its backward move to the inter-rib wall and the rib. The structure develops following the upstream rib and remains, in first instance, attached to it (*Figure 8 a)*). This recirculating structure impinges in the inter-rib wall, following a line almost parallel to the rib. This is clearly seen from the tracers shown for the horizontal plane  $Ixz$  (*Figure 9*). The size of the structure increases as it follows the “z” direction. This behavior can be appreciated when looking at the reattachment line, which diverges from the rib direction towards the downstream rib.

Downstream of the reattachment line, the flow has a little area before finding the downstream rib. It follows the main flow direction and starts to redevelop. For this pitch distance  $l/h=7.5$ , this redevelopment area is relatively small. Up to this position, the structure remained attached to the inter-rib wall and the upstream rib, but another recirculating structure starts to grow.

Following the rib direction, after the position of the plane  $Ixy$ , another concentration of streamlines in the plane  $Ixz$  can be appreciated near the upstream rib, as the footprints of the new vortical structure. The later rotates in an opposite direction of the main one, and contributes to detach the bigger structure from the inter-rib wall which keeps it confined between the upstream rib and the inter-rib wall. The results of plane  $2xy$  shows this phenomenon. The main structure is already separated from the rib, and the flow coming from the core of the channel does not impinge anymore in the inter-rib wall. When looking at the plane  $Ixz$ , the streamlines within the upstream sidewall and the position of the plane  $Ixy$  where concentrated in such a way to allow to define the reattachment line, diverge not towards the upstream rib, but to de downstream sidewall following “z” direction. This fact is also another reason to consider that the main structure is detaching from the inter-rib wall. As can be seen in from plane  $2xy$  (*Figure 7 and 8 b)*) the core of the structure is further from the inter-rib wall than in the position of the plane  $Ixy$ .

A third rotating structure is observed in front of the downstream rib, and rotates in the same direction than the main one. This structure is feed with the redeveloped fluid near the downstream sidewall, which finds itself deflected  $45^\circ$  by the presence of the rib. At the “z” position of the plane  $2xy$  both counter-rotating structures contribute to lift the main structure from the wall. Between the planes  $2xy$  and  $3xy$ , the main structure seems to be pushed over the rib height. The tracers in the plane  $1xz$  do not show a backward move that could denote recirculation anymore (*Figure 9*). At the same time, the main structure merges with the small one in front of the downstream rib. Since both are rotating in the same sense, they contribute to lift the flow over the downstream rib to jump to the next inter-rib space in the channel. In the pattern shown in the plane  $3xy$ , it can be seen that the structure only exists, as recirculating traces, close to the downstream rib. Looking at the same plane  $3xy$ , the counter-rotating structure behind the upstream rib can still be seen. The traces in plane  $1xz$  show its existence.

This structure merges with the core flow mixing the flow coming from the intersection of the rib with the inter-rib wall and the flow coming form the core of the channel. This structure remains rotating between the inter-rib wall and the downstream sidewall, getting confined between this sidewall and its intersection with the downstream rib by the flow directed trough the main structure that impinges against the downstream sidewall. Before this structure finds the downstream rib, it is lifted out of the inter-rib space by the action of the recirculating structure created in front of this rib.

In order to compare the flow projection on the measured planes, the *Figure 8, 9, 10* and *11* show a superposition of the streamtracers of the flow in dark color for the one ribbed wall planes and in lighter color for the two ribbed wall configuration.

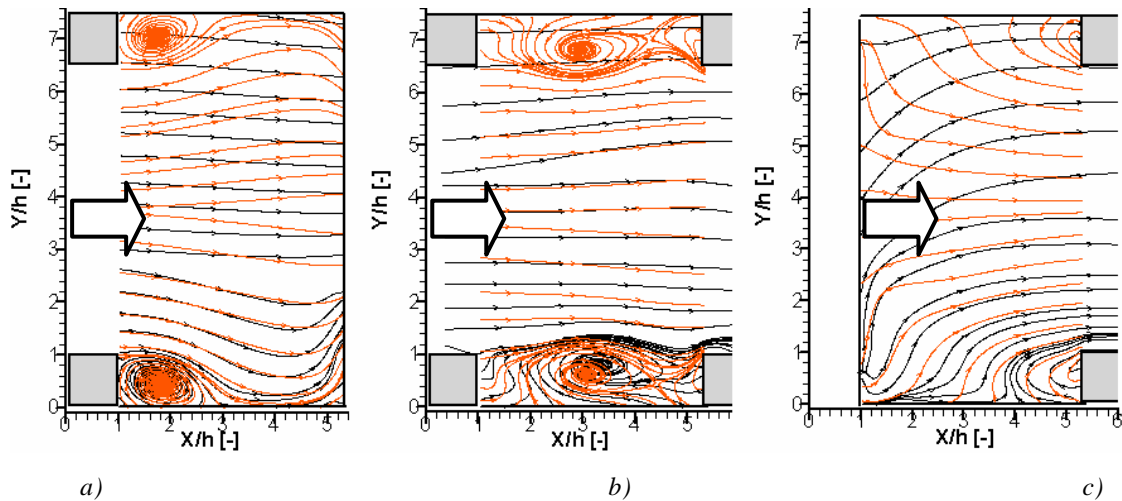


*Figure 8. Inter-rib flow field projection  $h=7.5$*

- a) Plane 1xy*
- b) Plane 2xy*
- c) Plane 3xy*

As shown in *Figure 7* and *Figure 8*, the flow behavior in the inter-rib space does not differ significantly for one and two ribbed walls. The most significant difference is due to the contraction and expansion experienced by the main stream over the ribs. For the two ribbed walls case this effect is, obviously, stronger due to the double blockage. It also results in the fact that the core of the main recirculating structure remains closer to the inter-rib wall (*Figure 8 a) and b)*). This will enhance the heat transfer process (as will be seen in the *Section 3.2*), but also produces an increase in the pressure losses introduced by the presence of the second ribbed wall (di Sante [15]).

Other difference between the one and two ribbed walls cases lays on the secondary flows induced inside the channel. The effect of the two structures rotating at the same induces a secondary movement divided in two horizontal cells (Chanteloup [16]), whereas the presence of just one ribbed wall creates a unique cell (Taslim [17]).

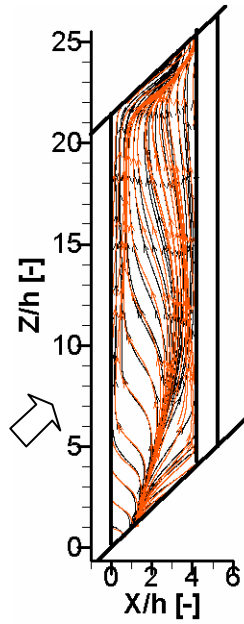
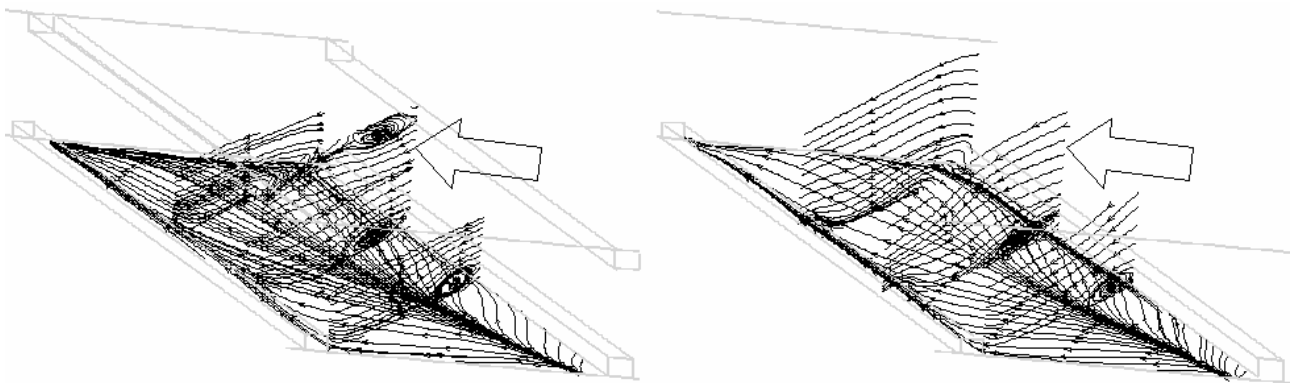


Figure 9. Inter-rib flow field projection, plane  $1xy$ ,  $\Delta/h=7.5$

*Pitch to rib height ratio 15*

The main flow characteristics were also determined in the configuration with a larger inter-rib distance (Figure 10): The recirculating structure behind the upstream rib dominates the flow behavior. The small counterrotating structure, located between the main structure and the upstream rib, interacts with the dominant structure pushing it away from the upstream rib. The streamwise rotational structure which appears in front of the downstream rib is another feature that can also be observed in this configuration. However it is not interacting with the main recirculating structure. Finally, the footprint of the corner structure between the inter-rib wall and the downstream sidewall is seen in the plane  $1xz$ , and links the counterrotating structure behind the upstream rib and the recirculation between the inter-rib wall and the downstream sidewall.



a)

b)

Figure 10. Inter-rib flow field projection  $\Delta/h=15$

a) Two ribbed walls

b) One ribbed wall

The main difference between the two configurations lays in the extension of the redeveloping area. Whereas, for the configurations of  $\Delta/h=7.5$  this area was reduced to the downstream corner of the upstream sidewall and the downstream rib, for  $\Delta/h=15$  this regions covers a larger area, almost the half of the inter-rib space between the reattachment line and

the downstream rib (Figure 12). Thus, the boundary layer redevelops along the surface until it finds the downstream rib and the small structure following its axis. In all zones, the fluctuating levels are reduced to the ones of the core flow within the ribbed walls (Figure 17).

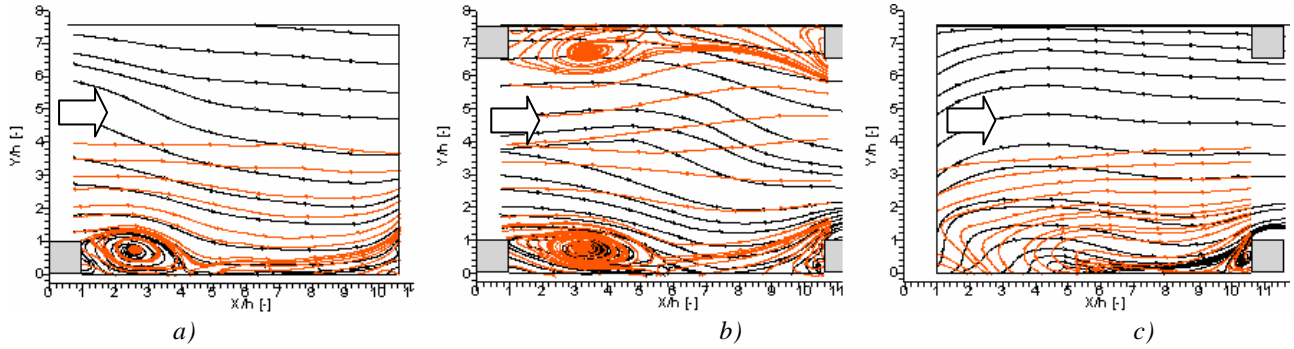


Figure 11. Inter-rib flow field projection  $p/h=15$   
 a) Plane 1xy  
 b) Plane 2xy  
 c) Plane 3xy

The main structure remains attached to the upstream rib over a longer distance. For this pitch distance, the presence of the small rotating structure in front of the downstream rib does not interact with it, so it does not contribute to lift and detach the bigger one from the inter-rib wall, as it was the case for the  $p/h=7.5$ . The redeveloped flow has more influence in the fading of this flow characteristic than it has in the smaller pitch to rib height distance configuration.

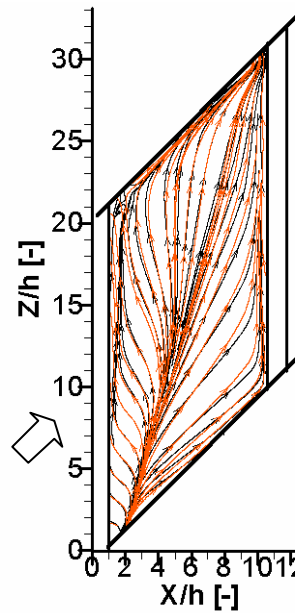


Figure 12. Inter-rib flow field projection, plane 1xy,  $p/h=15$

As for the previous configuration ( $p/h=7.5$ ), the coincidence of the streamtracers for both one and two ribbed walls configurations is remarkable (Figure 11 and Figure 12). Then, from the study of both cases, can be said that the presence of one ribbed wall or two ribbed walls in the channel does not affect the flow behavior in the space between two consecutive turbulence promoters.

### 3.3 Aero-thermal performance

The use of turbulence promoters in internal cooling channels provides a heat transfer coefficient higher than the one found for the smooth channels (Thiery [1]). This justifies to use ribs for increasing the heat exchange between the blade

and the coolant air. Several measurements of the heat transfer exchange on the ribbed wall have been performed at VKI by Thiery and Fedrizzi [16], [8], for a channel in similarity with the one used for the P.I.V. measurements with one and two ribbed walls.

The main difference between the two channels is that the ribbed walls are heated to simulate the cooling effect of the air aspirated through the channel. The technique used, T.L.C., allows mapping the enhancement factor and the surface averaged Nusselt number distribution in the inter-rib area.

#### *Pitch to rib height ratio 7.5*

The averaged Nusselt contour plots are shown in *Figure 13 a)* and *b)* for one and two ribbed walls respectively. Over the Nusselt contours, the streamlines for the plane  $lxz$  are superimposed to them. In this way the analysis of the cooling performance can be linked with the aerodynamic behavior of the flow.

As it was shown in the precedent section 3.2, the flow going over the rib reattaches close to the upstream lateral wall corner. For this reason the maximum of the heat transfer is found, for both one and two ribbed walls, in this corner of the inter-rib space. The fluid that enters in the recirculating structure is directed to the downstream sidewall following a spiral path. The wall heat transfer benefits from the exchange of momentum and energy between this recirculating structure and the shear flow behind the rib, creating a zone with the maximum values of  $Nu$ . The mean line of this high heat transfer zone diverges from the rib in the direction of the upstream sidewall, in a direction almost parallel to the reattachment line. Looking at the results of superimposed streamlines on the averaged Nusselt number contour plots, the reattachment line occurs slightly downstream of the peak observed for the heat transfer. This observation was also found by Shen et al. [13] for a channel with  $90^\circ$  ribs. The results corroborate the conclusions drawn by Çakan [3], who placed the reattachment line as a straight line in the mean zone where the maximum of heat transfer occurs.

A big difference in this feature of the cooling performance can be seen between the single ribbed wall channel and the double ribbed one. In the first case, the area of higher Nusselt number lies in form of a peak with its mean line situated slightly upstream of the reattachment line. In the second configuration, this area, apart from presenting higher values of Nusselt number, shows a shorter double peak with its second spike placed in the zone of redevelopment of the flow. This peak is created by the structure formed in front of the downstream rib.

As the recirculated fluid moves towards the downstream sidewall, the progressive contact between the flow and the inter-rib wall makes the convective heat exchange less efficient. The lower intensity of the fluctuations of the velocity (*Figure 17*) also contributes to lower the Nusselt number in this area. Between the recirculating structure and the upstream rib a narrow zone is filled with an almost stagnant fluid moving into the small counter-rotating vortex created downstream of the rib following its direction. Thus, a zone of lower heat transfer between the first rib and the recirculating structure can be appreciated, showing the lowest Nusselt number just before the corner between the upstream rib, the inter-rib wall and the downstream sidewall. Just in the corner, the start of the recirculating structure between the inter-rib wall and the sidewall increases the Nusselt number. This is due to the mixing of the flow with the cooler air coming from the core of the channel. Before reaching the downstream rib, this structure is lifted by the presence of the other structure formed in front of this rib and the redeveloped warmer fluid going towards this corner. Then a decrease in the Nusselt number can be seen in the corner of the downstream sidewall with the inter-rib wall and the downstream rib.

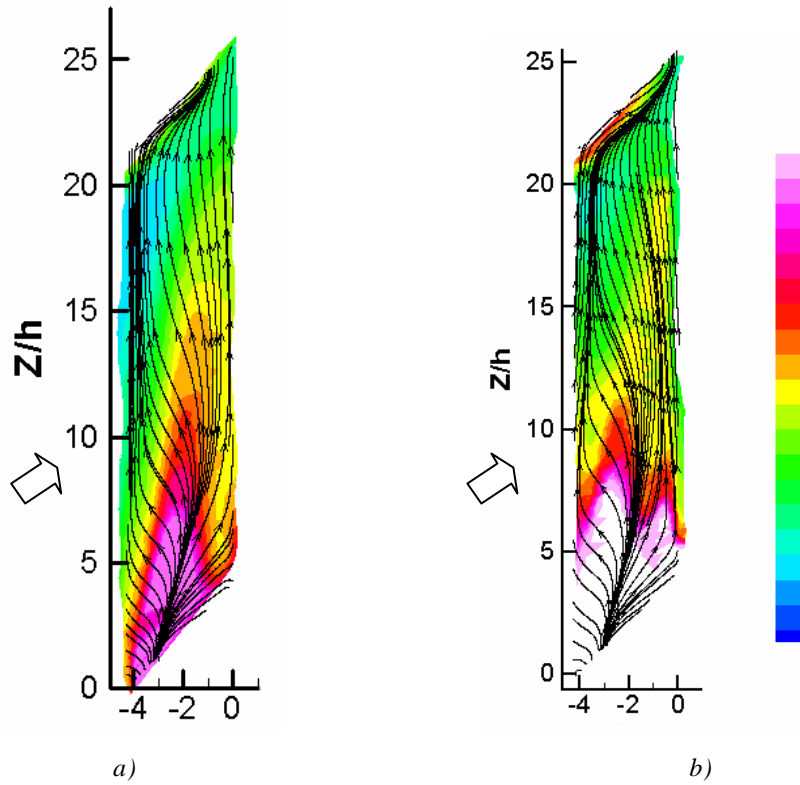


Figure 13. Inter-rib Nusselt number distribution and streamtracers ( $\gamma/h=7.5$ )  
 a) One ribbed wall  
 b) Two ribbed walls

The graphics in *Figure 14 a)* and *b)* show extracted profiles of  $Nu$  from the heat transfer contour plots at the position of the  $xy$  planes for the P.I.V. measurements, and the profiles of the  $u_{rms}xv_{rms}$  extracted from the P.I.V. measurements. It can be seen that the maximum of the product of the *rms* components of the velocity,  $u_{rms}$  and  $v_{rms}$  for the vertical planes  $1xy$  and  $2xy$ , takes place at a the beginning of the zone where the heat transfer reaches the maximum. The maximum level of fluctuations in the flow occurs closer to the center of the recirculating zone than to the impingement point. These profiles were taken at a distance of  $y/h=0.025$  from the bottom ribbed wall. The values of the fluctuations of the velocity for the planes  $3xy$  are too small to be able to relate them with the heat transfer process as it was with the planes  $1xy$  and  $2xy$ .

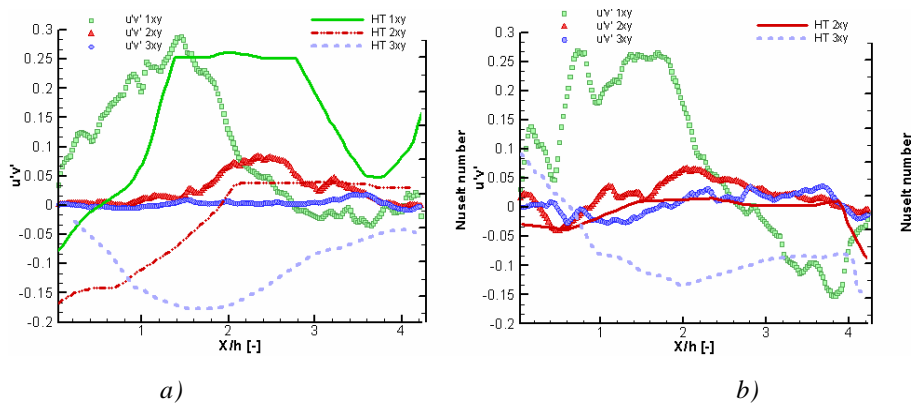


Figure 14. Extracted profiles of  $u_{rms}xv_{rms}$  for the vertical planes  $xy$  and their comparison with Nusselt number profiles, configuration  $\gamma/h=7.5$

- a) One ribbed wall
- b) Two ribbed walls

Pitch to rib height ratio 15

Considering the aerodynamic behavior, the main features that were seen in the configuration  $\tau/h=7.5$  were also found in the case of  $\tau/h=15$ . The same conclusions can be drawn for the heat transfer.

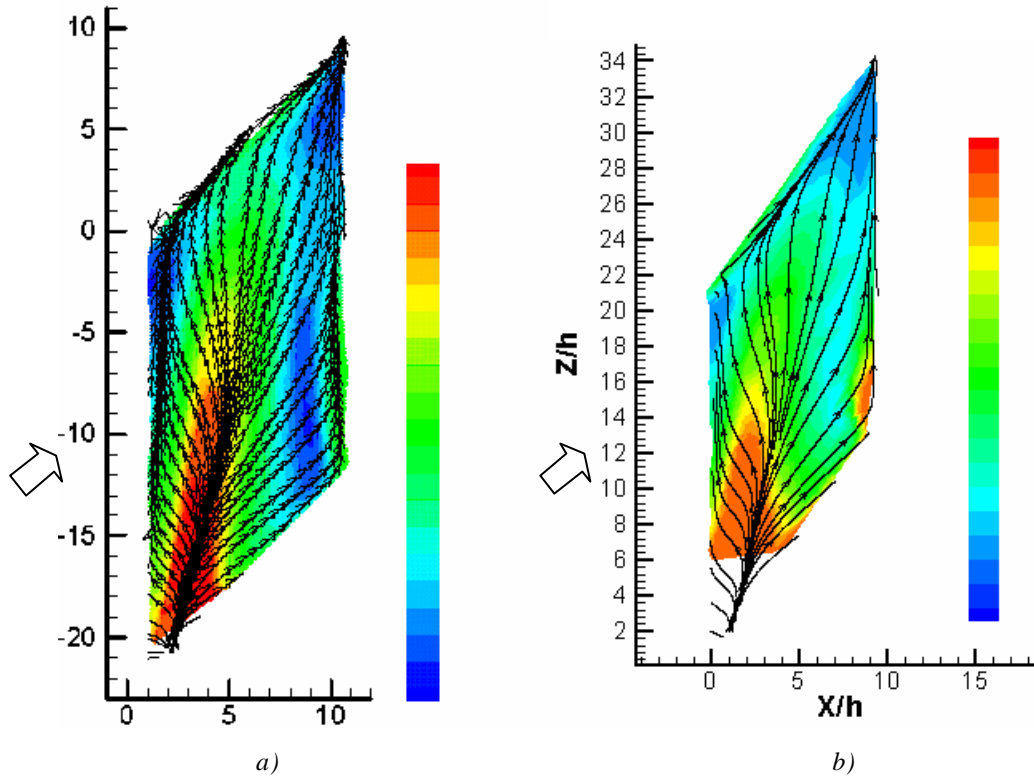


Figure 15. Inter-rib Nusselt number distribution and streamtracers ( $\tau/h=15$ )  
a) One ribbed wall  
b) Two ribbed walls

Again, the peak for the Nusselt number is seen upstream from the reattachment line (Figure 15 a) and b)), and it is sharper for the one ribbed wall configuration. The counterrotating structure creates a hotter area along the intersection of the upstream rib and the inter-rib wall. When reaching the junction with the downstream sidewall, the presence of the corner structure and the recirculating fluid along this intersection enhances slightly the heat transfer.

Downstream of the reattachment line, the flow has a longer distance until the next rib to redevelop. This fact decreases the Nusselt number in front of the downstream rib. Only the effect of the structure created in front of the rib increases the heat transfer process, but its efficiency is restricted to the area close to the intersection of the upstream sidewall and the downstream rib. At the intersection of the downstream rib with the downstream sidewall, the confluence of the reattached flow that is lifted to go over the next rib makes the heat exchange lower.

The fact that the two consecutive ribs are farther apart makes the heat exchange less homogeneous than for the smaller pitch. This implies an important gradient of temperature along the inter-rib space, and also between the upstream and the downstream sides of the same rib.

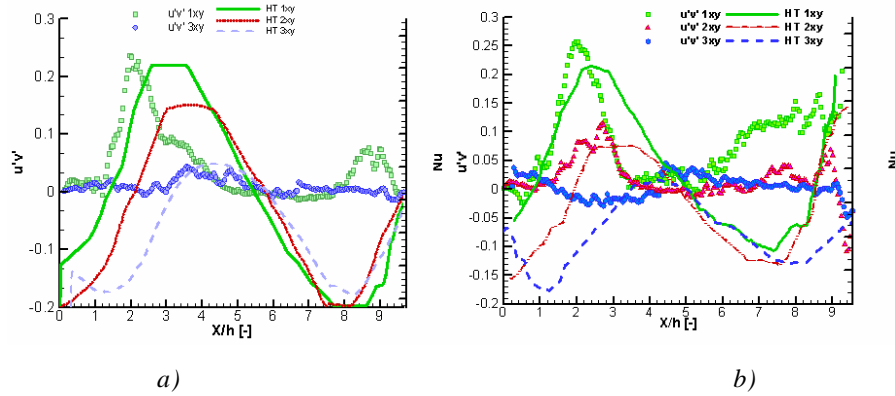


Figure 16. Extracted profiles of  $u_{rms}xv_{rms}$  for the vertical planes  $xy$  and their comparison with Nusselt number profiles, configuration  $\delta/h=15$

- a) One ribbed wall
- b) Two ribbed walls

A direct relation can also be observed between the product of the fluctuating components of the velocity,  $u_{rms}xv_{rms}$ , and the local Nusselt number in Figure 16. The peak of the fluctuations is located slightly upstream of the higher Nusselt number plateau, and as the flow redevelops, the product  $u_{rms}xv_{rms}$  reduces as the Nusselt number does. As the flow approaches the downstream rib, the fluctuation level increases and the heat transfer enhances again with a small delay in space. This fact is not seen for the extracted profiles from the plane 3xy, but also their heat transfer coefficient are lower.

### Velocity fluctuations

Figure 17 shows the square of the *rms* values for the velocity component in the  $x$  axis,  $u_{rms}x u_{rms}$  for both configurations  $\delta/h=7.5$  a) and  $\delta/h=15$  b) for the two ribbed walls cases. They emphasize the importance of the high level of the fluctuations in the heat transfer process and explain the use of the ribs not only for enlarging the surface exchange area but also as a way of increase the turbulence for the improvement of the heat transfer. Again the main structure is the responsible of this increase in the turbulence level of the flow. In the redevelopment areas, the fluctuations decrease to levels similar to the ones in the core flow. Also a slight higher value of these velocity fluctuations is observed for the configuration  $\delta/h=7.5$  showing the importance of increasing the number of ribs along the channel in order to enhance the turbulence level. As it was said before, the penalty for this enhancement is the increase of the pressure drop along the blade internal passages.

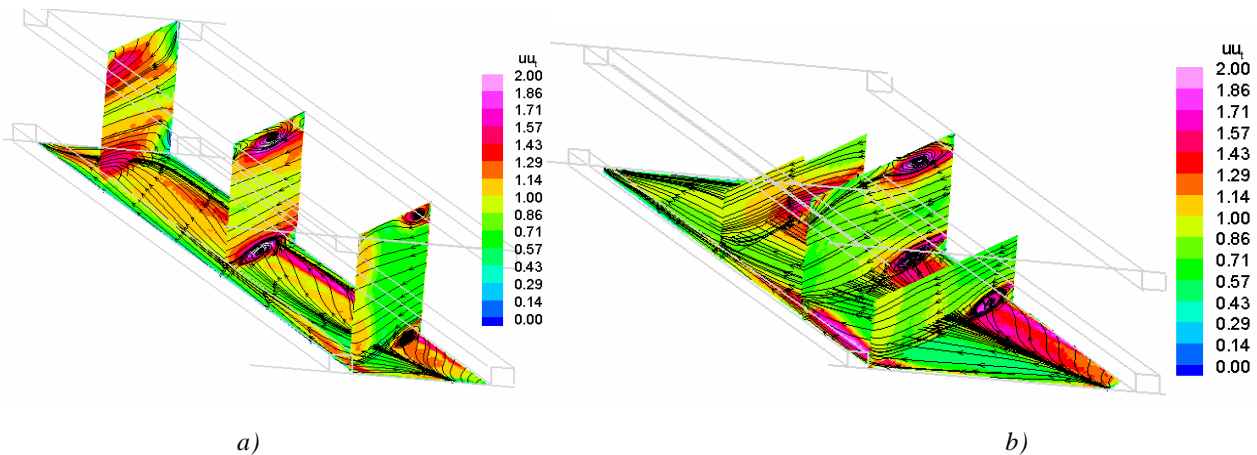


Figure 17.  $u_{rms}x u_{rms}$  contour plot (2 ribbed walls)

- a)  $\delta/h=7.5$
- b)  $\delta/h=15$

#### 4. SUMMARY

A three dimensional image of the flow within an inter-rib space for gas turbine cooling channel was measured for several configurations, varying the pitch to rib height ratio and the number of walls equipped with ribs. The main interest of this study is that these turbulence promoters are inclined at 45° with respect to the mean flow direction.

Some characteristics of the flow between two consecutive ribs are identified for both one and two ribbed wall configurations and for the two inter-rib distances:

- A dominating recirculating structure behind the upstream rib.
- A counterrotating small structure between the main one and the upstream rib.
- A streamwise rotating structure in front of the downstream rib.
- A corner structure between the inter-rib wall and the downstream sidewall.

Contour plots for the heat transfer distribution on the inter-rib wall were also investigated. The measurements were performed respecting geometrical and flow similarity conditions with respect to real turbine blades. The ensemble analysis of the Nusselt number maps and the flow streamlines points out the direct relation between the flow pattern and the heat transfer performance. Also, the areas of high transfer ratio are related to the velocity fluctuations extracted from the vertical planes.

#### REFERENCES

- [1] Thiry M. *Experimental investigation on aerodynamic and thermal performance of a gas turbine cooling channel with 45 degrees inclined ribs*, VKI Stagier Report 2001-03 7, 2001
- [2] Fedrizzi R. *Experimental investigation on thermal performance of a gas turbine two ribbed walls cooling channel with 45° inclined ribs*, VKI Stagier Report 2002, 2002
- [3] Çakan M. *Aero-thermal Investigation of Fixed Rib-roughened Internal Cooling Passages*, VKI-TN 2001-198, von Karman Institute, 2001
- [4] Casarsa L. *Aerodynamic Performance of a fixed rib-roughened internal cooling passage*, Universita degli Studi di Udine von Karman Institute for Fluid Dynamics, 2003
- [5] Riethmuller M.L., Lourenço L. *Optical measurements of velocity in particulate flows*, VKI Lecture Series: Laser velocimetry, VKI LS 1981-3, 1981
- [6] Scarano F., Riethmuller M.L. *Iterative multigrid approach in PIV image processing with discrete window offset*, *Experiments in Fluids*, 26, 513-523, 1999
- [7] Scarano F., Riethmuller M.L. *Advances in iterative multigrid PIV image processing*, *Experiments in Fluids*, Suppl., 51-60, 2000
- [8] Scarano F. *Particle Image Velocimetry development and application*, Universita Federico Secondo di Napoli, von Karman Institute for Fluid Dynamics, 2001
- [9] Kline S.J., McClintok F.A. *Describing uncertainties in single sample experiments*, *Mechanical Engineering Journal*, January, 1953
- [10] Rau G., Moeller D., Çakan M., Arts T., *The effects of the periodic ribs on the local aerodynamical and heat transfer performance of a straight cooling channel*, ASME 96-GT- 541, Sept. 1996
- [11] Arts T., Rau G., Çakan M., Vialonga J., Fernandez D., Garnowski F., Laroche E., *Experimental and numerical investigation of flow and heat transfer in large scale, turbine cooling representative, rib roughened channels*, 2nd European Conference on Turbomachinery-Fluid Dynamics and Thermodynamics, Antwerp, Belgium, March 5- 7 1997
- [12] Ligrani et al. *Comparison of heat transfer augmentation techniques*” *AIAA Journal* Vol 41, No. 3 March 2003

- [13] Shen J.R., Wang z., Ireland P.T., Jones T.V., Byerley A.R. *Heat transfer enhancement within a turbine blade cooling passage using ribs and combinations of ribs with film cooling holes*, *Journal of Turbomachinery*, Vol. 118, July 1996
- [14] Diette C., Arts T., *Application de la thermographie par cristaux liquides dans les cavites de refroidissement d'aubes de turbines* *Techniques experimentales en convection*, SFT, Mar. 2002
- [15] A. di Sante, *Aerodynamic study of turbine blade internal cooling channels*, VKI Stagier Report 2001, 2001
- [16] Chanteleup D., Boelcs A. *PIV Investigation of the Flow Characteristics in 2-Leg Internal Coolant Passages of Gas Turbine Airfoils*, 4th European Conference on Turbomachinery ATI-CST-031/01
- [17] Taslim M.E., *Convective cooling in non-rotating and rotating channels: Experimental aspects*. VKI Lecture Series 2000-03
- [18] Raffel M., Willert C., Kompenhans J. *Particle Image Velocimetry. A practical guide*, Springer Verlag, 1998
- [19] Arts T. et al., *Aero-thermal performance of internal cooling systems in turbomachines*, VKI Lecture Series 2000-03